Observation of flat electron temperature profiles in the Lithium Tokamak Experiment

D.P. Boyle,[1,*] R. Majeski,[1] J.C. Schmitt,[1,2] C. Hansen,[3] R. Kaita,[1] S. Kubota,[4] M. Lucia,[1] and T.D. Rognlien[5]

[1] *Princeton Plasma Physics Laboratory, Princeton, New Jersey 08543, USA*
[2] *Physics Department, Auburn University, Auburn, Alabama 36849, USA*
[3] *Department of Aeronautics and Astronautics, University of Washington, Seattle, Washington 98195, USA*
[4] *Institute of Plasma and Fusion Research, University of California, Los Angeles, California 90095, USA*
[5] *Lawrence Livermore National Laboratory, Livermore, California 94551, USA*

(Dated: May 15, 2017)

It has been predicted for over a decade that low-recycling plasma facing components in fusion devices would lead to high edge temperatures and flat or nearly flat temperature profiles. In recent experiments with lithium wall-coatings in the Lithium Tokamak Experiment (LTX), a hot edge (>200 eV) and flat electron temperature profiles have been measured following the termination of external fueling. Reduced recycling was demonstrated by retention of ∼60% of the injected hydrogen in the walls following the discharge. Electron energy confinement followed typical ohmic confinement scaling during fueling, but did not decrease with density after fueling terminated, ultimately exceeding the scaling by ∼200%. Achievement of the low-recycling, hot edge regime has been an important goal of LTX and lithium plasma facing component research in general, as it has potentially significant implications for the operation, design, and cost of fusion devices.

PACS numbers:

The use of lithium as a wall material in fusion devices has the potential to enable a fundamentally different operating regime [1–3] than the conventional approach based on high-recycling, high-density, low-temperature detached divertors. Chemical bonding of hydrogen isotopes by lithium (Li) can reduce wall-recycling and edge neutral density, avoiding the low edge temperature boundary condition imposed by the influx of cold neutrals. By severing the link from the cold wall to the hot core, Li has been predicted to allow high edge temperatures with flat or nearly flat temperature profiles, with fusion production in the entire confined volume and suppression of temperature gradient driven instabilities leading to improved confinement [1–3]. A regime with greatly reduced neoclassical transport has also been predicted in the absence of thermal gradients [4]. Even with thermal gradients, a high edge temperature can greatly improve fusion gain, with core temperature approximately proportional to edge temperature in marginally ion temperature gradient stable profiles [5, 6].

Improved confinement would enable more compact fusion devices with lower capital cost, and risks of costly downtime and repairs to the plasma facing components (PFCs) could also be reduced by lithium walls. While the conventional high-density, low-temperature divertor concept is motivated by spreading heat loads to avoid thermal damage to solid materials and reduce erosion and impurity influx by sputtering [7], lithium would naturally be liquid in a fusion device, making it robust to damage with the ability to handle large heat loads. Sufficiently thick Li PFCs could also prevent tritium retention in solid materials where it is difficult to extract and can require maintenance. Liquid Li PFCs would continuously flow out of a reactor for fuel extraction (and possibly heat removal, with fast flow) before being returned. Several concepts for extraction of tritium from lithium have been proposed [8, 9], though large scale extraction from liquids remains an open challenge perhaps larger than trace retention in solids [9–11].

Lithium is also attractive because of its low first ionization potential, meaning sputtered Li will ionize close to the wall and redeposit rather than entering the confined plasma as an impurity. Lithium's low atomic number Z=3 also means relatively large Li impurity concentrations would be tolerable in a fusion device. In the conventional, low-temperature edge regime, material sputtering increases with edge temperature. However, sputtering yield for Li peaks at $T_e \sim 200$ eV and then decreases with edge temperature [12], making a high-temperature, low-density edge feasible with a lithium wall.

Experiments using lithium coatings have shown a variety of performance improvements, mainly attributed to reduced recycling. Improved density control and H/D ratio were achieved in EAST due to pumping of the dominant plasma species by Li [13]. NSTX demonstrated higher edge rotation, likely because Li reduced neutrals and therefore charge exchange drag [14]. Li coatings also led to greatly improved confinement in TFTR, CDX-U, NSTX, and DIII-D [15–18]. NSTX, EAST [19], and DIII-D [18] also saw modification and suppression of edge-localized modes (ELMs), explained in NSTX by the change in recycling that modified and stabilized pedestal profiles [17, 20]. Methods to reduce edge neutrals without Li can also cause beneficial changes to the pedestal, reducing pedestal density and collisionality and changing the bootstrap current and density pedestal structure in C-Mod, JET, and AUG [21–23]. In both NSTX and the devices without Li, peeling-ballooning stability improved, allowing a higher temperature and pressure pedestal and improving confinement [24–26].

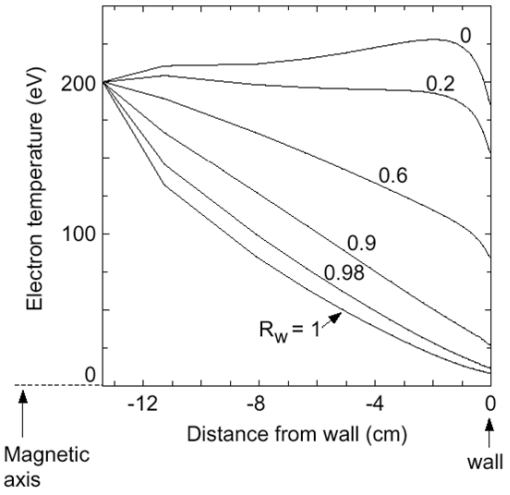

FIG. 1. Electron temperature T_e profiles from UEDGE simulations as a function of global wall recycling coefficient R_w (ratio of incoming wall neutrals to outgoing plasma ions). In the simulations, core temperature and density were held fixed at 200 eV and 5×10^{13} cm^{-3}. Particle diffusivity was set at 0.5 m^2/s and thermal diffusivities were 1 m^2/s.

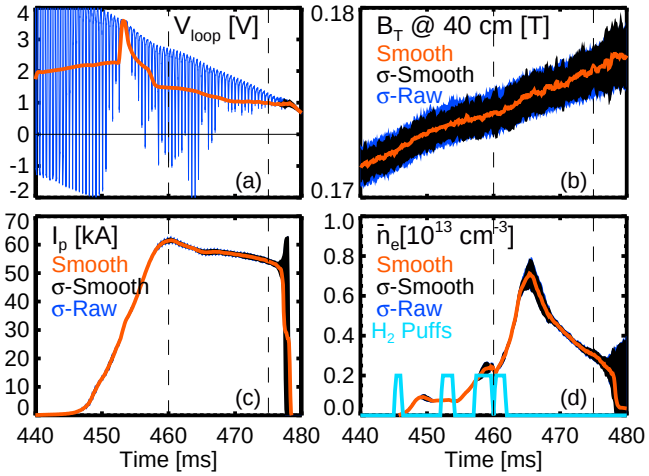

FIG. 2. Waveforms of (a) loop voltage V_{loop}, (b) toroidal field B_T, (c) plasma current I_p, and (d) line-averaged density $\bar{n}_e$. The red line is the median over the 55 discharges of the time-smoothed waveforms, the black band is the standard deviation of the smoothed waveforms, and the blue band is the standard deviation of the raw waveforms. The gas puffing control signal (cyan) is overlaid in (d). The vertical dashed lines indicate the part of the discharge when Thomson scattering measurements were made and TRANSP modelling performed.

While no previous experiment has directly measured the hot edge, flat temperature profile, low-recycling regime, modeling of TFTR improved confinement discharges was consistent with many of the key predictions of the low-recycling theory [1, 2]. Modeling based on gyrofluid and gyrokinetic turbulence simulations showed that improved confinement in TFTR supershots could be explained by higher temperatures in the outer part of the plasma (attributed to reduced recycling; the edge was not directly measured) leading to reduced ion temperature gradient turbulence and improved confinement [5, 27].

Predictive modeling studying variation of the global wall recycling coefficient has previously been performed with the UEDGE multi-fluid edge code [28], using parameters relevant to the present work. The UEDGE simulations are consistent with the low-recycling theory, predicting a strong increase in edge temperature with flattened temperature profiles when most escaping ions do not return as cold neutrals (Figure 1). In this Letter, we present the first experimental observation of flat electron temperature profiles with a hot edge in the Lithium Tokamak Experiment (LTX), the first step in exploring this promising regime.

The LTX device is a spherical tokamak [29] designed and built specifically to study Li PFCs [30]. In early experiments using neutral helium to disperse solid Li coatings, significant improvement in performance was shown. Neutral pressure and residual gas analyzer measurements showed high pumping and retention of the fueling gas [31, 32], and reduced recycling was inferred from Lyman-α measurements and interpretive modeling with the DEGAS2 neutrals code [33, 34]. Later experiments with electron-beam evaporation showed additional improvements, including good performance using liquid lithium coatings [35, 36]. Using the Materials Analysis and Particle Probe (MAPP) to make *in vacuo* measurements, it was determined that while the surface was mostly oxidized within a few hours, the solid lithium coatings were still effective at pumping hydrogen [37–39].

In the LTX vacuum vessel, a close fitting shell surrounds ∼80% of the plasma surface, with toroidal and poloidal breaks dividing the shell into 4 quadrants. The shell is 1 cm thick copper with a 1.5 mm thick stainless steel liner providing a lithium-compatible PFC. For the experiments described here, ∼150-200 mg of Li was evaporated from each side, giving coatings ∼75-100 nm thick assuming uniform coverage. The shell was allowed to cool overnight and discharges were performed the following day [40].

A series of 55 reproducible discharges were repeated with identical programming during a single run day (Figure 2). As the LTX Thomson scattering system [41, 42] can measure electron density and temperature profiles only once per discharge, repeated discharges were necessary to measure time evolution of the plasma profiles. The vessel was pre-filled with 8×10^{-5} Torr of H_2, and breakdown occurred at t ∼445 ms. The pre-programmed waveform of the ohmic heating central solenoid induced the plasma current (I_p) with a peak value of ∼60 kA at 460 ms that decreased slightly over the next ∼17 ms before the discharge terminated. Additional fueling was

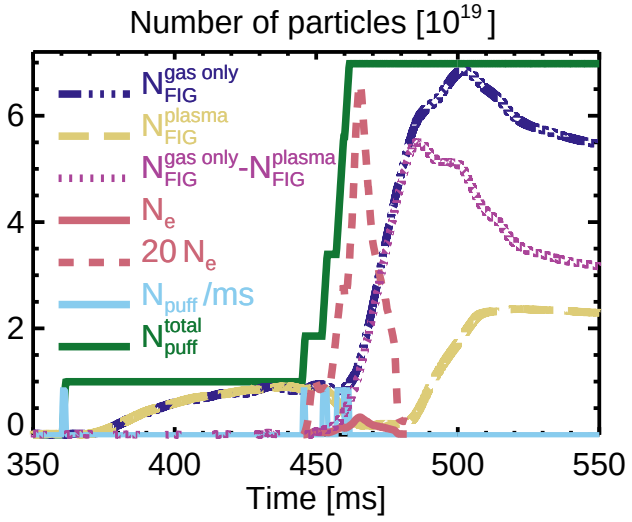

FIG. 3. Neutral hydrogen atom inventory from fast ion gauge (FIG) waveform without plasma (dark blue dot-dashed), with plasma (yellow dashed), and the difference (purple dotted). Electron inventory from interferometer and reconstructed plasma geometry (pink), and scaled by a factor of 20 (pink dashed). Fueling rate from high-field side gas puffer (cyan) and integrated fueling (green).

provided from the high-field side puffer, including a large puff beginning at the I_p peak. There was no additional fueling after the I_p peak, allowing study of the plasma with recycling as the only source of neutral gas.

As Li readily pumps hydrogen atoms and ions, but not molecular hydrogen, one simple indicator of reduced recycling due to the Li coatings was the reduction in vessel neutral pressure after the discharges terminated, relative to calibration shots taken throughout the day with identical gas fueling but no plasma [31, 32]. In Figure 3, the dark blue dot-dashed curve shows the averaged neutral pressure for the gas-only shots, as measured with a vessel fast-ion gauge, while the yellow dashed curve shows the averaged neutral pressure for the plasma discharges. During the discharge, the neutral pressure was greatly reduced as the particles were confined in the plasma volume and retained in the walls. When the discharge terminated, the plasma recombined to molecular hydrogen, and in the absence of wall retention, the vessel pressure would return to the gas-only value. The difference in vessel pressure between the gas-only and plasma shots, shown in purple dots, gives the amount of hydrogen retained in the walls, equivalent to 60% of the hydrogen puffed to fuel the plasma.

Thomson scattering (TS) was the key diagnostic in the present study. The LTX TS ruby laser fired a single 15-20 J, ∼35 ns pulse per discharge on a near-radial midplane path [41, 42]. Light was imaged using downward viewing optics onto an array of optical fibers, and 11 channels covering the radial midplane from the magnetic axis outboard were measured with a spectrometer and intensified camera. The TS measurement time was varied over the 55 repeated discharges in 1 ms intervals covering the period from 460-477 ms, with measurements at each time point repeated several times. In order to improve signal-to-noise, the raw spectra were averaged for all TS measurements taken at the same time point, as well as their nearest neighbors in time [40]. The measurement time of averaged spectra was taken to be the average of the the measurement times. The TS density (n_e) profiles were mapped to the high-field side of the magnetic axis, fit with smoothing splines, numerically integrated, and normalized to the line-averaged density $\bar{n}_e$. $\bar{n}_e$ was measured with a 1 mm microwave interferometer [43] along a radial midplane beam path that reflected off the center stack. For an initial normalization, the mapping was performed based on the plasma boundary as determined directly with flux loops and mirnov coils [32, 44] and an analytic formula for the Shafranov shift [45]. The TS profiles of electron pressure p_e, and an assumption for ion pressure $p_i = 0.3p_e$ were used to constrain magnetic equilibrium reconstructions using PSI-Tri. PSI-Tri is an axisymmetric equilibrium code that includes a model for eddy currents induced in the thick copper shell as well as the vacuum vessel [46]. Final n_e normalizations using the magnetic reconstructions for mapping were only slightly changed from the initial normalizations. The TS profiles were also used to calculate ADAS [47] photo-emission coefficients for visible spectroscopic measurements of impurity density profiles. Using a simple model for the unmeasured impurity charge states, these measurements indicated fairly low impurity concentrations, with $\sim 2-4\%$ lithium, $\sim 0.6-2\%$ carbon, $\sim 0.4-0.7\%$ oxygen, and $Z_{eff} < 1.2$ [40, 48].

Figure 4 shows n_e, T_e, and p_e profiles near the peak density from the large gas puff (t = 465 ms, left) and long after external gas fueling was terminated at (t = 474 ms, right). Though 11 radial points were measured, the three farthest outboard were unreliable due to low count rates and are not shown. The accuracy of the TS profiles are corroborated by comparison of the n_e profiles with those measured with a profile reflectometer [49, 50]. The major radii of magnetic axis and last closed flux surface (LCFS) at the outer midplane are shown as vertical lines, calculated using the PSI-Tri equilibria and the flux loop measurements.

The determination of the LCFS in LTX had some uncertainties, but the observation that the T_e profile remained flat from the core to the edge after external fueling was terminated is robust to several different methods of interpretation. Later in the discharge, the radius of the outboard midplane LCFS determined solely using magnetics was ∼5 cm less than that determined using the TS-constrained reconstruction. This difference means that T_e remained above 200 eV for ∼3 cm beyond the plasma edge at the LCFS determined using the magnetics-only

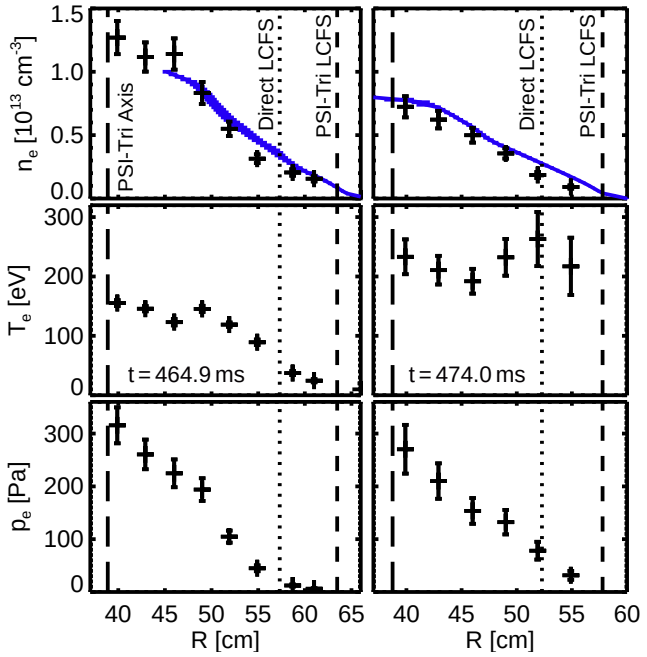

FIG. 4. Thomson scattering (TS) n_e, T_e, and p_e profiles during the peak of the gas puff (left) and after fueling ceased (right). The magnetic axis and last closed flux surface (LCFS) from magnetic reconstructions are shown as vertical dashed lines, while the LCFS from direct magnetic measurements are shown as vertical dotted lines. Reflectometer n_e profiles (blue) are overlaid on the TS n_e profiles.

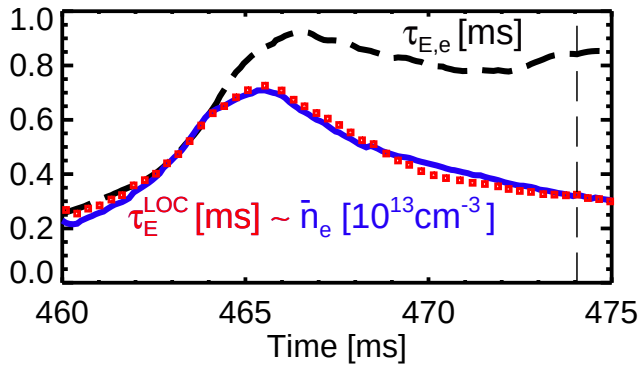

FIG. 5. Electron energy confinement time $\tau_{E,e}$ from TRANSP (black dashed) and the neo-Alcator Linear Ohmic Confinement (LOC) scaling τ_E^{LOC} (red dotted) in units of ms; line-averaged density $\bar{n}_e$ (blue) in units of 10^{13} cm^{-3}. In cgs units, $\tau_E^{LOC} = 7.1 \times 10^{-22} \bar{n}_e a_{eff}^{1.04} R_0^{2.04} q^{0.5}$ [52]. After fueling was terminated and density decreased, $\tau_{E,e}/\tau_E^{LOC}$ increased to ~3 as the T_e profile became flat at t = 474 ms (vertical dashed line).

measurement, while the farthest outboard point was still ~2 cm inside the TS-constrained boundary measurement. The TS and reflectometer both showed a gradually decreasing n_e profile, with no evidence of the sharp edge density gradient seen in the standard high-confinement regime (the H-mode pedestal). Based on the TS-constrained LCFS measurement, a sharp temperature drop inside the LCFS cannot be completely excluded. However, a hypothetical T_e pedestal would imply a transport barrier that confined energy but not particles such as I-mode [51], which has not been previously observed in a tokamak operating without auxiliary heating, at low aspect ratio, or with a limiter rather than a divertor.

The main transport mechanisms in LTX and the importance of temperature gradient driven modes relative to other effects are not presently well characterized. Furthermore, analysis of the transport of these discharges is difficult due to the transient nature of the discharges, with large changes in density and temperature and small but significant variations in loop voltage, toroidal field, and plasma current (shown in Figure 2 (a-c)) as well as reductions in major and minor radius (shown in Figure 4). Still, initial transport analysis using the TRANSP code [40, 53] to calculate electron energy confinement time $\tau_{E,e}$ is encouraging. Figure 5 shows the time evolution of $\tau_{E,e}$ calculated by TRANSP over the interval $t = 460 - 475$ ms based on the averaged TS profiles, PSI-Tri equilibria, and measured magnetic coil waveforms. As expected for an ohmic tokamak, $\tau_{E,e}$ increased proportionally to density during the gas puff. However, $\tau_{E,e}$ then remained nearly constant even as density decreased below half of the peak value at the time the flat T_e profile was observed. During the initial density increase, electron confinement was well described by the neo-Alcator Linear Ohmic Confinement (LOC) scaling (cgs units) $\tau_E^{LOC} = 7.1 \times 10^{-22} \bar{n}_e a_{eff}^{1.04} R_0^{2.04} q^{0.5}$ [52], though $\tau_{E,e}$ increased to $1.3\tau_E^{LOC}$ at peak density. R_0 ~39 cm is the major radius of the magnetic axis, a_{eff} ~27 cm is the effective minor radius of the elongated torus, and q ~7 is the edge magnetic field safety factor. Curiously, though perhaps coincidentally, $\tau_{E,e}$ began to exceed $\tau_E^{LOC} \sim 10^{-16} \bar{n}_e$ just after density exceeded the Saturated Ohmic Confinement critical density scaling ($n_e^{crit} \sim 5 \times 10^{12}$ cm^{-3}), which typically leads to reduced confinement [54]. After fueling was terminated and density decreased, $\tau_{E,e}/\tau_E^{LOC}$ further increased to ~3 as the T_e profile became flat.

Given the longstanding predictions of flat temperature profiles with low recycling PFCs from theory and modeling, the experimental confirmation of the temperature profile predictions is striking. The dramatic change in the T_e profile from peaked to flat following the termination of external fueling suggests that the PFCs did not continue to provide a steady source of cold neutrals, but rather retained hydrogen, as independently measured by a fast ion gauge. The achievement of such flat T_e profiles was a major goal of LTX and gives evidence for a new, potentially high performance plasma regime for fusion devices. This regime will be studied further in the

upcoming LTX-β [48], which will include the addition of a neutral beam and enhancements to enable longer discharges. Core fueling with a neutral beam will provide auxiliary heating and allow the density to remain stationary in the low recycling regime without edge fueling, enabling well-controlled studies of the effects of this regime on confinement.

The authors thank E.Merino, T. Kozub, C.M. Jacobson, B.P. LeBlanc, R.E. Bell, T.M. Biewer, T.K. Gray, F. Scotti, and all past and present members of the LTX Team for their work, especially developing the Thomson scattering system, LTX TRANSP analysis, spectroscopy, and general machine operations. This work was supported by US Department of Energy contracts DE-AC02-09CH11466, DE-AC05-00OR22725, and DE-AC52-07NA27344.

* dboyle@pppl.gov

[1] S. I. Krasheninnikov, L. E. Zakharov, and G. V. Pereverzev, Physics of Plasmas **10**, 1678 (2003).
[2] L. E. Zakharov, N. Gorelenkov, R. White, S. I. Krasheninnikov, and G. V. Pereverzev, Fusion Engineering and Design **72**, 149 (2004).
[3] R. B. White, in *The Theory of Toroidally Confined Plasmas* (Imperial College Press, London, 2014) 3rd ed., pp. 447–456.
[4] P. J. Catto and R. D. Hazeltine, Physics of Plasmas **13** (2006), 10.1063/1.2403090.
[5] M. Kotschenreuther, W. Dorland, M. A. Beer, and G. W. Hammett, Physics of Plasmas **2**, 2381 (1995).
[6] A. M. Dimits, G. Bateman, M. A. Beer, B. I. Cohen, W. Dorland, G. W. Hammett, C. Kim, J. E. Kinsey, A. H. Kritz, L. L. Lao, J. Mandrekas, W. M. Nevins, S. E. Parker, A. J. Redd, D. E. Shumaker, R. Sydora, and J. Weiland, Physics of Plasmas **7**, 969 (2000).
[7] S. I. Krasheninnikov, A. S. Kukushkin, and A. A. Pshenov, Physics of Plasmas **23**, 055602 (2016).
[8] L. Olson, B. Garcia-Diaz, H. Colon-Mercado, J. Teprovich, and D. Babineau, *Direct LiT Electrolysis in a Metallic Fusion Blanket*, Tech. Rep. (Savannah River Site (SRS), Aiken, SC (United States), 2016).
[9] M. Ono, M. Jaworski, R. Kaita, Y. Hirooka, and T. Gray, Fusion Engineering and Design **117**, 124 (2017).
[10] R. Nygren and F. Tabarés, Nuclear Materials and Energy **9**, 6 (2016).
[11] F. Tabarés, E. Oyarzabal, A. Martin-Rojo, D. Tafalla, A. de Castro, and A. Soleto, Nuclear Fusion **57**, 016029 (2017).
[12] J. Laszlo and W. Eckstein, Journal of Nuclear Materials **184**, 22 (1991).
[13] Z. Sun, J. Hu, G. Zuo, J. Ren, B. Cao, J. Li, D. Mansfield, and the EAST team, Fusion Engineering and Design **89**, 2886 (2014).
[14] D. K. Mansfield, H. W. Kugel, R. Maingi, M. G. Bell, R. E. Bell, R. Kaita, J. Kallman, S. M. Kaye, B. P. LeBlanc, and D. Mueller, Journal of Nuclear Materials **390-391**, 764 (2009).
[15] D. K. Mansfield, K. W. Hill, J. D. Strachan, M. G. Bell, S. D. Scott, R. Budny, E. S. Marmar, J. A. Snipes, J. L. Terry, S. Batha, R. E. Bell, M. Bitter, C. E. Bush, Z. Chang, D. S. Darrow, D. Ernst, E. D. Fredrickson, B. Grek, H. W. Herrmann, A. Janos, D. L. Jassby, F. C. Jobes, D. W. Johnson, L. C. Johnson, F. M. Levinton, D. R. Mikkelsen, D. Mueller, D. K. Owens, H. K. Park, A. T. Ramsey, A. L. Roquemore, C. H. Skinner, T. N. Stevenson, B. C. Stratton, E. J. Synakowski, G. Taylor, A. von Halle, S. von Goeler, K. L. Wong, and S. J. Zweben, Physics of Plasmas **3**, 1892 (1996).
[16] R. Majeski, R. P. Doerner, T. Gray, R. Kaita, R. Maingi, D. K. Mansfield, V. A. Soukhanovskii, J. Spaleta, J. Timberlake, and L. E. Zakharov, Physical Review Letters **97**, 075002 (2006).
[17] R. Maingi, D. Boyle, J. Canik, S. Kaye, C. Skinner, J. Allain, M. Bell, R. Bell, S. Gerhardt, T. Gray, M. Jaworski, R. Kaita, H. Kugel, B. Leblanc, J. Manickam, D. Mansfield, J. Menard, T. Osborne, R. Raman, A. Roquemore, S. Sabbagh, P. Snyder, and V. Soukhanovskii, Nuclear Fusion **52**, 083001 (2012).
[18] T. Osborne, G. Jackson, Z. Yan, R. Maingi, D. Mansfield, B. Grierson, C. Chrobak, A. McLean, S. Allen, D. Battaglia, A. Briesemeister, M. Fenstermacher, G. McKee, and P. Snyder, Nuclear Fusion **55**, 063018 (2015).
[19] J. Li, H. Y. Guo, B. N. Wan, X. Z. Gong, Y. F. Liang, G. S. Xu, K. F. Gan, J. S. Hu, H. Q. Wang, L. Wang, L. Zeng, Y. P. Zhao, P. Denner, G. L. Jackson, A. Loarte, R. Maingi, J. E. Menard, M. Rack, and X. L. Zou, Nature Physics **9**, 817 (2013).
[20] D. P. Boyle, R. Maingi, P. B. Snyder, J. Manickam, T. H. Osborne, R. E. Bell, and B. P. LeBlanc, Plasma Physics and Controlled Fusion **53**, 105011 (2011).
[21] J. Hughes, A. Loarte, M. Reinke, J. Terry, D. Brunner, M. Greenwald, A. Hubbard, B. LaBombard, B. Lipschultz, Y. Ma, S. Wolfe, and S. Wukitch, Nuclear Fusion **51**, 083007 (2011).
[22] L. Frassinetti, M. Beurskens, S. Saarelma, J. Boom, E. Delabie, J. Flanagan, M. Kempenaars, C. Giroud, P. Lomas, L. Meneses, C. Maggi, S. Menmuir, I. Nunes, F. Rimini, E. Stefanikova, H. Urano, and G. Verdoolaege, Nuclear Fusion **57**, 016012 (2017).
[23] M. G. Dunne, S. Potzel, F. Reimold, M. Wischmeier, E. Wolfrum, L. Frassinetti, M. Beurskens, P. Bilkova, M. Cavedon, R. Fischer, B. Kurzan, F. M. Laggner, R. M. McDermott, G. Tardini, E. Trier, E. Viezzer, and M. Willensdorfer, Plasma Physics and Controlled Fusion **59**, 014017 (2017).
[24] J.-S. Lönnroth, V. Parail, D. McDonald, S. Saarelma, E. de la Luna, and M. Beurskens, Nuclear Fusion **51**, 013003 (2011).
[25] R. Maingi, Nuclear Fusion **54**, 114016 (2014).
[26] E. Wolfrum, M. Beurskens, M. Dunne, L. Frassinetti, X. Gao, C. Giroud, J. Hughes, T. Lunt, R. Maingi, T. Osborne, M. Reinke, and H. Urano, Nuclear Materials and Energy **0**, 1 (2017).
[27] D. R. Ernst, B. Coppi, S. D. Scott, and M. Porkolab, Physical Review Letters **81**, 2454 (1998).
[28] T. D. Rognlien, P. N. Brown, R. B. Campbell, T. B. Kaiser, D. A. Knoll, P. R. McHugh, G. D. Porter, M. E. Rensink, and G. R. Smith, Contributions to Plasma Physics **34**, 362 (1994).
[29] M. Ono and R. Kaita, Physics of Plasmas **22**, 040501

(2015).
[30] R. Majeski, L. Berzak, T. Gray, R. Kaita, T. Kozub, F. M. Levinton, D. Lundberg, J. Manickam, G. V. Pereverzev, K. Snieckus, V. A. Soukhanovskii, J. Spaleta, D. Stotler, T. Strickler, J. Timberlake, J. Yoo, and L. E. Zakharov, Nuclear Fusion **49**, 055014 (2009).
[31] D. P. Lundberg, *Princeton University*, Ph.D. thesis, Princeton University (2012).
[32] J. C. Schmitt, T. Abrams, L. R. Baylor, L. Berzak Hopkins, T. Biewer, D. Bohler, D. Boyle, E. Granstedt, T. Gray, J. Hare, C. M. Jacobson, M. Jaworski, R. Kaita, T. Kozub, B. Leblanc, D. P. Lundberg, M. Lucia, R. Maingi, R. Majeski, E. Merino, A. Ryou, E. Shi, J. Squire, D. Stotler, C. E. Thomas, K. Tritz, L. Zakharov, L. B. Hopkins, T. Biewer, D. Bohler, D. Boyle, E. Granstedt, T. Gray, J. Hare, C. M. Jacobson, M. Jaworski, R. Kaita, T. Kozub, B. Leblanc, D. P. Lundberg, M. Lucia, R. Maingi, R. Majeski, E. Merino, A. Ryou, E. Shi, J. Squire, D. Stotler, C. E. Thomas, K. Tritz, and L. Zakharov, Journal of Nuclear Materials **438**, S1096 (2013).
[33] E. M. Granstedt, *Princeton University*, Ph.D. thesis, Princeton University (2013).
[34] D. Stotler and C. Karney, Contributions to Plasma Physics **34**, 392 (1994).
[35] K. Tritz, R. E. Bell, P. Beiersdorfer, D. Boyle, J. Clementson, M. Finkenthal, R. Kaita, T. Kozub, S. Kubota, M. Lucia, R. Majeski, E. Merino, J. Schmitt, and D. Stutman, Plasma Physics and Controlled Fusion **56**, 125014 (2014).
[36] J. C. Schmitt, R. E. Bell, D. P. Boyle, B. Esposti, R. Kaita, T. Kozub, B. P. LeBlanc, M. Lucia, R. Maingi, R. Majeski, E. Merino, S. Punjabi-Vinoth, G. Tchilingurian, A. Capece, B. Koel, J. Roszell, T. M. Biewer, T. K. Gray, S. Kubota, P. Beiersdorfer, K. Widmann, and K. Tritz, Physics of Plasmas **22**, 056112 (2015).
[37] M. J. Lucia, *Princeton University*, Ph.D. thesis, Princeton University (2015).
[38] M. Lucia, R. Kaita, R. Majeski, F. Bedoya, J. Allain, T. Abrams, R. Bell, D. Boyle, M. Jaworski, and J. Schmitt, Journal of Nuclear Materials **463**, 907 (2015).
[39] R. Kaita, M. Lucia, J. P. Allain, F. Bedoya, R. Bell, D. Boyle, A. Capece, M. Jaworski, B. E. Koel, R. Majeski, J. Roszell, J. Schmitt, F. Scotti, C. H. Skinner, and V. Soukhanovskii, Fusion Engineering and Design **117**, 135 (2017).
[40] D. P. Boyle, *Princeton University*, Ph.D. thesis, Princeton University (2016).
[41] T. Strickler, R. Majeski, R. Kaita, and B. P. LeBlanc, Review of Scientific Instruments **79**, 10E738 (2008).
[42] C. M. Jacobson, *Princeton University*, Ph.D. thesis, Princeton University (2014).
[43] L. Porte, C. L. Rettig, W. A. Peebles, and X. Ngyuen, Review of Scientific Instruments **70**, 1082 (1999).
[44] L. F. Berzak, *Princeton University*, Ph.D. thesis, Princeton University (2010).
[45] J. P. Freidberg, *Ideal Magnetohydrodynamics* (Plenum Press, 1987) p. 489.
[46] C. Hansen, D. P. Boyle, J. C. Schmitt, and R. Majeski, Physics of Plasmas **24**, 042513 (2017), arXiv:arXiv:1701.05851.
[47] H. P. Summers, "The ADAS User Manual, version 2.6," (2004).
[48] R. Majeski, R. E. Bell, D. P. Boyle, R. Kaita, T. Kozub, B. P. LeBlanc, M. Lucia, R. Maingi, E. Merino, Y. Raitses, J. C. Schmitt, J. P. Allain, F. Bedoya, J. Bialek, T. M. Biewer, J. M. Canik, L. Buzi, B. E. Koel, M. I. Patino, A. M. Capece, C. Hansen, T. Jarboe, S. Kubota, W. A. Peebles, and K. Tritz, Physics of Plasmas **24**, 056110 (2017).
[49] S. Kubota, X. V. Nguyen, W. A. Peebles, L. Zeng, E. J. Doyle, and A. L. Roquemore, Review of Scientific Instruments **72**, 348 (2001).
[50] S. Kubota, R. Majeski, W. A. Peebles, R. E. Bell, D. P. Boyle, R. Kaita, T. Kozub, M. Lucia, E. Merino, X. V. Nguyen, T. L. Rhodes, and J. C. Schmitt, Review of Scientific Instruments **88**, 053502 (2017).
[51] D. G. Whyte, A. E. Hubbard, J. W. Hughes, B. Lipschultz, J. E. Rice, E. S. Marmar, M. Greenwald, I. Cziegler, A. Dominguez, T. Golfinopoulos, N. Howard, L. Lin, R. M. McDermott, M. Porkolab, M. L. Reinke, J. Terry, N. Tsujii, S. Wolfe, S. Wukitch, and Y. Lin, Nuclear Fusion **50**, 105005 (2010).
[52] R. J. Goldston, Plasma Physics and Controlled Fusion **26**, 87 (1984).
[53] R. J. Hawryluk, "An Empirical Approach to Tokamak Transport," (1981).
[54] ITER Physics Expert Groups on Confinement and Transport and Confinement Modelling and Database, Nuclear Fusion **39**, 2175 (1999).